Research Article | Vol. 28, No. 26 / 21 December 2020 / Optics Express 39750
Optics EXPRESS

Noise and distortion analysis of dual frequency comb photonic RF channelizers

CALLUM DEAKIN[1,2] AND ZHIXIN LIU[1,3]

[1]Department of Electronic and Electrical Engineering, University College London, London, UK
[2]callum.deakin.17@ucl.ac.uk
[3]zhixin.liu@ucl.ac.uk

Abstract: Dual frequency combs are emerging as highly effective channelizers for radio frequency (RF) signal processing, showing versatile capabilities in various applications including Fourier signal mapping, analog-to-digital conversion and sub-sampling of sparse wideband signals. Although previous research has considered the impact of comb power and harmonic distortions in individual systems, a rigorous and comprehensive performance analysis is lacking, particularly regarding the impact of phase noise. This is especially important considering that phase noise power increases quadratically with comb line number. In this paper, we develop a theoretical model of a dual frequency comb channelizer and evaluate the signal to noise ratio limits and design challenges when deploying such systems in a high bandwidth signal processing context. We show that the performance of these dual comb based signal processors is limited by the relative phase noise between the two optical frequency combs, which to our knowledge has not been considered in previous literature. Our simulations verify the theoretical model and examine the stochastic noise contributions and harmonic distortion, followed by a broader discussion of the performance limits of dual frequency comb channelizers, which demonstrate the importance of minimizing the relative phase noise between the two frequency combs to achieve high signal-to-noise ratio signal processing.

1. Introduction

The ability to detect high bandwidth signals accurately is an essential tool for science, with applications in wireless and optical communications, radar systems, and defense technologies. The relentless growth of global communications traffic in particular has driven demand for systems operating at high (e.g. >10 GHz) radio frequencies (RF), where the design of electronic and optoelectronic devices, along with the associated high bandwidth analog and digital circuitry, becomes extremely challenging.

One strategy to address this challenge is to decompose fast signals to many parallel slow signals using RF channelizers. RF channelizers spectrally slice the incoming high bandwidth signal to a number of low bandwidth signals, so that the low bandwidth (sub-band) signals can be detected by a bank of lower bandwidth (and therefore lower noise) detectors. Since this technique relaxes the bandwidth requirements of the sub-band detection components such as photodiodes, RF filters, and analog-to-digital converters (ADCs), it can enable accurate and efficient detection of high bandwidth signals by using a bank of low frequency components.

Photonic approaches to channelize RF signals have been the subject of many research efforts due to the wide available bandwidth and insusceptibility to electromagnetic interference, and bolstered by the rapid progress in integrated photonic technology [1]. The general concept is that an incoming high bandwidth RF signal is cast onto multiple optical wavelengths (e.g. from a frequency comb source) which can be separated to perform the channelization. One technique, inspired by dual frequency comb spectroscopy [2–4], utilizes the Vernier effect between two

#410340 https://doi.org/10.1364/OE.410340
Journal © 2020 Received 16 Sep 2020; revised 13 Nov 2020; accepted 14 Nov 2020; published 16 Dec 2020

Optics EXPRESS

optical frequency combs of different spacing to down-convert the spectral slices to baseband [5–7]. Reported demonstrations of dual frequency comb channelization for RF signal processing include sub-noise signal detection [8,9], OFDM reception [10], photonic assisted analog-to-digital conversion (ADC) [11–13] and wideband RF disambiguation of sparse signals [14], with a variety of comb generation techniques used including electro-optic modulation, parametric mixing and micro ring resonators. The performance of these dual-comb RF signal processors have been characterised in different ways in the individual systems. Although it has been identified that factors including the power and phase noise of the frequency comb, harmonic distortion of the optical modulator, and photodiode noise can degrade the fidelity of the channelized signal, no existing literature to our knowledge has performed a rigorous, generalised analysis of how noise and distortion scales in a dual frequency comb based RF channelizer.

In this paper, we assess the fundamental performance limitations of the dual comb channelizer in the context of RF signal processing applications. We present a theoretical framework to assess the noise characteristics of any dual frequency comb channelizer, accounting for phase noise, photodiode noise, ADC noise and modulator harmonic distortion, which is agnostic to the comb generation technique. The theoretical predictions are verified against numerical simulations based on parameters representative of our previous experiments. We show that aside from the nonlinearity/photodiode noise trade-off, the dual comb method is particularly sensitive to the relative phase noise between the two frequency combs. Achieving either a low absolute phase noise or high degree of correlation between the two combs is therefore critical to achieving low noise channelization with the dual comb method, especially at high frequencies.

2. Noise and distortion model

The essence of the dual comb technique is that the beating between two frequency combs of different spacing can down convert an optical response recorded on either comb to lower RF frequencies that are determined by the difference between the spacing of the two combs. This is known as the Vernier effect in analogy to its mechanical equivalent [15,16] and is illustrated in Fig. 1.

In the context of signal processing, one frequency comb of spacing f_{sig} (the 'signal comb') can be modulated with the input RF signal so that it is copied onto every comb line. This means that the second frequency comb (the 'local oscillator (LO) comb') of spacing $f_{LO} = f_{sig} + \Delta f$ will act as a set of local oscillators offset from the baseband of the original signal by $n\Delta f$ in the n-th comb line, provided that the comb lines of both frequency combs can be separated by an optical demutliplexer (e.g. an arrayed waveguide grating) for parallel coherent reception. Ideally, the spacing of the optical demultiplexer should be matched to the LO comb spacing to prevent filter roll-off reducing the power of the detected signal in the higher channels.

Figure 2 shows a generic dual frequency comb RF channelizer architecture with noise and distortion sources highlighted. Two optical frequency combs with angular frequency spacing ω_{sig} and ω_{LO} are generated, one of which is modulated with the input signal, before individual comb lines are filtered optically. Each sub-channel can then be detected by a low speed coherent receiver and filtered to the subchannel bandwidth Δf by low pass filters, following by signal processing and digitisation. Note that for the numerical results presented this paper, we use cascaded phase and intensity modulators to generate our frequency combs without loss of generality. The models presented here can be equally applied to other comb generating techniques, such as parametric and microresonator combs [17–19], provided that the phase noise characteristics of the device is known.

We consider four fundamental sources of noise and distortion as highlighted in Fig. 2, and label the SNR limits they impose:

1. **Frequency comb phase noise**, SNR_{pn}. Each generated frequency comb will have two independent sources of phase noise: the seed laser phase noise, $\phi_0(t)$, and the phase

Optics EXPRESS

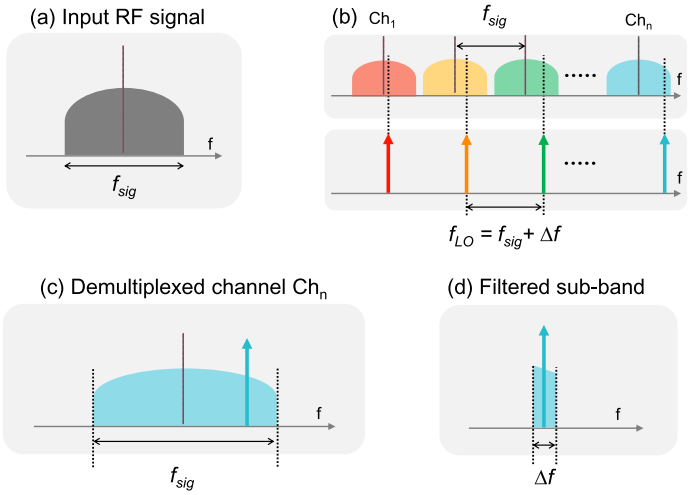

Fig. 1. Spectral slicing using dual optical frequency combs. (a) The input RF signal is (b) modulated onto a frequency comb of space f_{sig} that is mixed with a frequency comb of spacing $f_{LO} = f_{sig} + \Delta f$ to exploit the Vernier effect in the frequency domain. (c) The demultiplexed n-th channel, i.e. Ch$_n$ in (b), (d) is coherently detected and filtered in parallel with the other channels to obtain a Δf slice of the input signal.

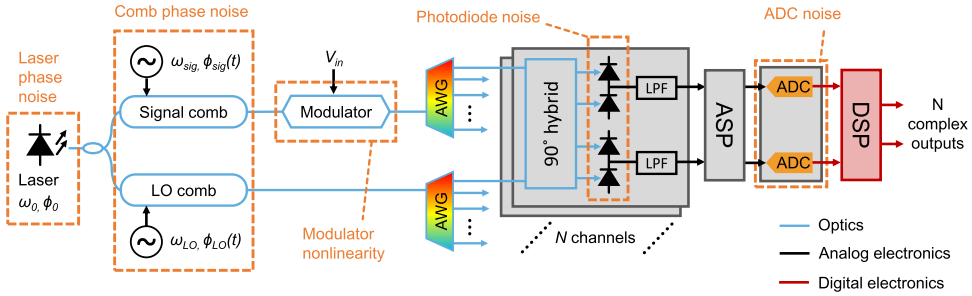

Fig. 2. A generic dual comb channelizer scheme, with noise and distortion sources highlighted. The LO comb and signal comb plus modulator paths are length matched to suppress the laser phase noise. Note that the order of the AWG and 90 degree hybrid may be switched. AWG, arrayed waveguide grating; ADC, analog to digital converter; LPF, low pass filter; ASP, analog signal processing; DSP, digital signal processing.

noise added during the comb generation, $\phi_{sig}(t)$ and $\phi_{LO}(t)$, for the signal and LO comb, respectively. We do not consider amplitude noise in either case since for most oscillators its impact is orders of magnitude lower than the phase noise [20] and can be effectively suppressed [21,22].

2. **Photodiode noise**, consisting of shot (SNR$_{sh}$) and thermal (SNR$_{th}$) noise. Dark noise is negligible compared to the shot noise in the dual comb system since the photodiodes are always illuminated by the local oscillator comb.

3. **Modulator nonlinearity**, SNR$_{mod}$. The electro-optic modulator that maps the input signal onto the signal comb will have some degree of nonlinearity, depending on the modulator design and the driving conditions, that will cause harmonic distortion. Unlike the stochastic

Optics EXPRESS

noise sources, this nonlinearity is deterministic and can be mitigated through highly linear modulator design or digital signal processing [23–28].

4. **ADC noise**, SNR_{ADC}. Each sub channel will be ultimately limited by the ADC noise if it is digitised. At MHz sampling rates and above, ADCs are typically limited by quantisation noise and clock jitter induced sampling error [29].

These noise/distortion sources are independent and so can be calculated separately to determine the level of noise that each source contributes. Furthermore, since the modulator nonlinearity is deterministic, we separate it from the stochastic noise processes to firstly define the signal to noise ratio without harmonics (SNR)

$$\mathrm{SNR} = \left(\mathrm{SNR}_{pn}^{-1} + \mathrm{SNR}_{sh}^{-1} + \mathrm{SNR}_{th}^{-1} + \mathrm{SNR}_{ADC}^{-1}\right)^{-1}. \tag{1}$$

The SNR limit imposed by harmonic distortions, SNR_{mod}, is often referred to as total harmonic distortion (THD). Together SNR and THD result in a signal to noise and disortion ratio (SINAD), which is the key figure of merit thoughout this paper

$$\mathrm{SINAD} = \left(\mathrm{SNR}_{pn}^{-1} + \mathrm{SNR}_{sh}^{-1} + \mathrm{SNR}_{th}^{-1} + \mathrm{SNR}_{ADC}^{-1} + \mathrm{SNR}_{mod}^{-1}\right)^{-1}. \tag{2}$$

2.1. Phase noise

We first analyze the phase noise limited SNR of the dual comb system shown in Fig. 2, considering only phase noise from the seed laser and the two comb generators. The output of a continuous wave laser with amplitude A_0, phase noise $\phi_0(t)$ and angular frequency ω_0 is given by

$$E_0(t) = A_0 e^{i(\omega_0 t + \phi_0(t))}. \tag{3}$$

A frequency comb can be generated using a multitude of different approaches. For example, in our previous demonstration the combs were generated by modulating the laser output [11,30], yielding phase noise that scales linearly with number of tones [31]. Note that this is the general property of a number of comb generation approaches including parametric combs and microresonator combs [32]. Consequently, we can assume without losing generality that the added phase noise to the n-th tone of the signal and LO combs are $n\phi_{sig}(t)$ and $n\phi_{LO}(t)$, respectively. The angular frequency between adjacent tones is $\omega_{sig}, \omega_{LO}$. This results in the optical field of the signal and LO combs for frequency combs with $2N + 1$ tones being

$$E_{sig}(t) = \sum_{n=-N}^{N} 2\sqrt{P_{sig,n}} e^{i((\omega_0 + n\omega_{sig})t + \phi_0(t) + n\phi_{sig}(t))}, \tag{4}$$

$$E_{LO}(t) = \sum_{n=-N}^{N} 2\sqrt{P_{LO,n}} e^{i((\omega_0 + n\omega_{LO})t + \phi_0(t) + n\phi_{LO}(t))} \tag{5}$$

where $P_{sig,n}$, $P_{LO,n}$ is the power of the n-th line in the signal comb and local oscillator comb respectively. Any loss in the optical paths can be accounted for by reducing the value of P_{sig} and P_{LO}. As per the dual comb RF signal processor shown in Fig. 2, the signal comb $E_{sig}(t)$ is passed through a Mach Zehnder modulator (MZM) biased at the null that is modulated with the RF signal under test. Initially, we treat the dual comb channelizer as a linear time invariant system

Optics EXPRESS

and consider the case of a sinusoidal input

$$V_{in}(t) = A_{in} \sin \omega_{in} t \tag{6}$$

and assume that the transfer function of the modulator, $M(V_{in}(t))$, is linear,

$$M(V_{in}(t)) = \sin\left(\frac{\pi V_{in}(t)}{V_\pi}\right) \approx \frac{\pi V_{in}(t)}{V_\pi}. \tag{7}$$

This is a valid approximation for a Mach-Zehnder modulator biased at the null if $V_{in} \ll V_\pi$, and we ignore insertion loss since this can be accounted for by a reduction in P_{sig}. Every comb line is therefore modulated with the input signal scaled by the ampltiude of the input signal and relative to the V_π of the modulator

$$\frac{\pi A_{in}}{V_\pi} \sin \omega_{in} t \cdot E_{sig} = \frac{\pi A_{in}}{V_\pi} \sin \omega_{in} t \sum_{n=-N}^{N} 2\sqrt{P_{sig,n}} e^{i((\omega_0 + n\omega_{sig})t + \phi_0(t) + n\phi_{sig}(t))}. \tag{8}$$

Now both frequency combs are optically filtered using an arrayed waveguide grating or other method of spacing ω_{LO} so that each comb line is separated for both frequency combs, and the n-th comb lines from each frequency comb can then be used as the inputs for an ideal optical coherent receiver. Assuming that the signal and LO paths are length matched, the balanced receivers yield the output currents

$$I_{I,n}(t) = 2R\sqrt{P_{sig,n}P_{LO,n}} \frac{\pi A_{in}}{V_\pi} \sin \omega_{in} t \cdot \mathrm{Re}\left\{e^{-i\cdot n(\Delta\omega t + \phi_{LO}(t) - \phi_{sig}(t))}\right\}, \tag{9}$$

$$I_{Q,n}(t) = 2R\sqrt{P_{sig,n}P_{LO}, n} \frac{\pi A_{in}}{V_\pi} \sin \omega_{in} t \cdot \mathrm{Im}\left\{e^{-i\cdot n(\Delta\omega t + \phi_{LO}(t) - \phi_{sig}(t))}\right\} \tag{10}$$

where R is the responsivity of the photodiodes and defining $\Delta\omega = \omega_{LO} - \omega_{sig}$. This can be summed to produce the full sub-band signal for the n-th channel

$$I_{out,n} \propto I_{I,n} + iI_{Q,n} = 2R\sqrt{P_{sig,n}P_{LO,n}} \frac{\pi A_{in}}{V_\pi} \sin \omega_{in} t \cdot e^{-in(\Delta\omega t + \phi_{LO}(t) - \phi_{sig}(t))}. \tag{11}$$

If an ideal low pass filter (LPF) of bandwidth $\frac{\Delta\omega}{2}$ is applied to the I and Q components then the output in the n-th channel is

$$I_{out,n} \propto R\sqrt{P_{sig}P_{LO}} \frac{\pi A_{in}}{V_\pi} e^{i(\omega_{in} - n\Delta\omega)t - n(\phi_{LO}(t) - \phi_{sig}(t))} \tag{12}$$

for $|\omega_{in} - n\Delta\omega| < \frac{\Delta\omega}{2}$. This is a complex valued sinusoid that is the analytic representation of the original input V_{in}, shifted in frequency by $-n\Delta\omega$ in the n-th sub-band and scaled by a constant, which will also include any gain experienced during the current to voltage conversion process. Since our analysis so far has been linear, it can easily be extended to arbitrary input signals, as described in the Appendix. Essentially, the n-th channel detects all frequencies in the range $\omega_{in} \pm \frac{\Delta\omega}{2}$.

This output signal has phase noise that is equal to the relative phase noise between the two corresponding comb lines, denoted $\Delta\phi_n(t) = n(\phi_{LO}(t) - \phi_{sig}(t))$. Since $\Delta\phi_n(t)$ is small we can

Optics EXPRESS

use the truncated Taylor expansion of e^x to write

$$e^{i(\omega_{in}-n\Delta\omega)t-\Delta\phi_n(t))} \approx (1 - i\Delta\phi_n(t))e^{i(\omega_{in}-n\Delta\omega)t} \tag{13}$$

and can see that the total noise power resulting from the relative phase noise for n-th tone is

$$\frac{1}{\mathrm{SNR}_{pn}} = \overline{\Delta\phi_n^2} = 2\int_0^{\frac{\Delta\omega}{2}} S_{\Delta\phi_n}(\omega)\mathrm{d}\omega \tag{14}$$

where $S_{\Delta\phi_n}(\omega)$ is the one sided power spectral density of $\Delta\phi_n$ which describes the spectral distribution of the down converted carrier in the n-th channel [33], defined as

$$S_{\Delta\phi_n}(\omega) = |n(\phi_{LO}(\omega) - \phi_{sig}(\omega))|^2 \tag{15}$$

and is integrated to the channel bandwidth [34] in (14). This phase noise spectrum contains contributions from both combs, so will depend on the phase noise level on each comb and how well this noise is correlated. If the frequency combs are uncorrelated, then the $\phi_{LO}(\omega)$ and $\phi_{sig}(\omega)$ are considered as independent phase noise and the power of the total phase noise is a simply sum of the two independent noise powers. However in this paper, we consider the fact that the phase noise of the two combs is likely to be correlated to some degree, and write them as being composed of a correlated part $\phi_c(\omega)$ and uncorrelated parts $\phi_{u,LO}(\omega)$ and $\phi_{u,sig}(\omega)$

$$\phi_{sig}(\omega) = k_{sig}(\omega)\phi_c(\omega) + \phi_{u,sig}(\omega), \tag{16}$$

$$\phi_{LO}(\omega) = k_{LO}(\omega)\phi_c(\omega) + \phi_{u,LO}(\omega) \tag{17}$$

where $k_{sig}(\omega)$, $k_{LO}(\omega)$ are functions describing the mapping of the correlated phase noise component between the repetition rate of each frequency comb [35]. This description is illustrated in Fig. 3. For example, if each comb is generated by electro-optic modulation using sinusoidal signals referenced to the same oscillator through an ideal phase locked loop (PLL) based synthesizer, $k_{sig}(\omega)$ and $k_{LO}(\omega)$ are simply equal to the PLL counter setting with any noise added by the PLL itself (or subsequent amplifiers) contributing to the uncorrelated parts $\phi_{u,sig}(\omega)$, $\phi_{u,LO}(\omega)$. Plugging this into (15) gives

$$S_{\Delta\phi_n}(\omega) = n^2\Big[|k_{LO}(\omega) - k_{sig}(\omega)|^2|\phi_c(\omega)|^2 + |\phi_{u,LO}(\omega)|^2 + |\phi_{u,sig}(\omega)|^2\Big]. \tag{18}$$

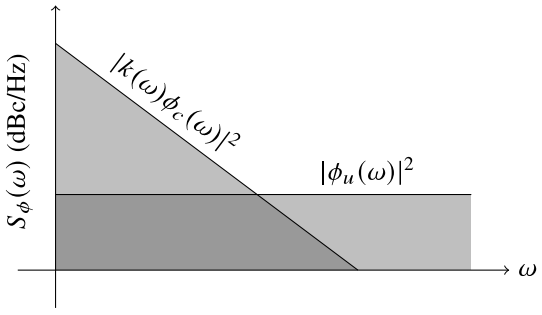

Fig. 3. Representative phase noise spectrum (ω plotted in log scale) of a given frequency comb pair in a dual comb system. The phase noise will consist of two parts: a correlated part $\phi_c(\omega)$ transformed by some function $k(\omega)$, and an uncorrelated part $\phi_u(\omega)$.

The phase noise power in the n-th channel consists of three parts: the correlated phase noise scaled by some factor $|k_{LO}(\omega) - k_{sig}(\omega)|^2$ describing the relationship between the two comb

Optics EXPRESS

synthesizers, and two contributions from the uncorrelated phase noise of the comb generators, all scaled by the square of the channel number n^2. For the purpose of our analysis, we further define the relative root-mean-square jitter in seconds σ_j

$$\sigma_j = \sqrt{\left(\frac{\overline{\Delta\phi_c}}{\Delta\omega}\right)^2 + \left(\frac{\overline{\Delta\phi_{u,sig}}}{\omega_{sig}}\right)^2 + \left(\frac{\overline{\Delta\phi_{u,LO}}}{\omega_{LO}}\right)^2} \tag{19}$$

which expresses the phase noise power (14) in seconds rather than radians, by summing the correlated and uncorrelated phase noise power contributions.

Here we have implicitly assumed in (9)/(10) that the optical path length of each comb is matched and therefore that the laser phase noise $\phi_0(t)$ will be perfectly cancelled at the coherent receiver. In reality, some amount of path length mismatch may occur, but we expect it to have a negligible contribution to the overall phase noise with a narrow linewidth laser source, which is discussed in the Appendix.

The extent to which the phase noise can be correlated is highly dependent on the comb synthesis technique. If each comb is generated by electro-optic modulation, then the driving signals are likely to be generated from the same reference oscillator through a phase locked loop (PLL) based synthesizer. In this case, the close-in phase noise (i.e. within the PLL loop bandwidth) will likely exhibit strong correlation [35], becoming uncorrelated at higher frequencies from carrier, where the phase noise will be contributed mainly from the internal circuitry of the synthesizer. Parametric combs seeded from electro-optic combs will generally exhibit similar characteristics [36].

On the other hand, frequency combs synthesised in microcavity resonators derive their phase noise (in addition to the pump laser phase noise) primarily from the thermorefractive fluctuations of the resonator [37,38]. Furthermore, optical-to-RF noise conversion via higher order chromatic dispersion and the frequency dependent quality factor of the resonator may facilitate additional decoherence of the comb lines [39].

2.2. Photodiode noise

Before calculating the photodiode noise limited SNR expressions, we first remark that the signal power of the sine wave (9)/(10) is given by half of the amplitude squared

$$P_{out} = \frac{4R^2 P_{sig,n} P_{LO,n} \pi^2 A_{in}^2}{V_\pi^2}. \tag{20}$$

We can assume that $P_{sig} \ll P_{LO}$, since the loss in the signal branch (modulation loss and modulator insertion loss) ensures that the local oscillator comb power is significantly higher than the signal comb and so is the dominant source of shot noise. This allows for the calculation of shot noise limited SNR, where q is the elementary charge

$$\mathrm{SNR}_{sh} \approx \frac{4R\pi^2 A_{in}^2}{V_\pi^2} \frac{P_{sig,n}}{q\Delta f}. \tag{21}$$

This is just the standard coherent receiver shot noise limit with the mean modulated signal power [40]. We can also write the thermal noise limited SNR

$$\mathrm{SNR}_{th} = \frac{R^2 P_{sig,n} P_{LO,n} \pi^2 A_{in}^2 R_L}{k_B T \Delta f V_\pi^2} \tag{22}$$

where R_L is the load resistance, k_B is the Boltzmann constant and T is the temperature in Kelvin. This gives the thermal noise limited SNR. Since the thermal noise power does not depend on the optical power, thermal noise limits the SNR when the optical power is low.

Optics EXPRESS

2.3. Modulator linearity

In (8), we approximated the modulator transfer function as linear. To determine how hard we can drive the modulator before we experience appreciable generation of harmonics we need to consider the actual nonlinear transfer function of a Mach-Zehnder modulator biased at the null, which is a sinusoid $M(V_{in}(t)) = \sin\left(\frac{\pi V_{in}(t)}{V_\pi}\right)$. For a single sinusoid input, multiplying E_{sig} by the full transfer function and using the Jacobi–Anger expansion gives

$$M(V_{in}(t))E_{sig} = 2\sum_{j=1}^{\infty} J_{2j-1}\left(\frac{\pi A_{in}}{V_\pi}\right)\sin[(2j-1)\omega_{in}t] \tag{23}$$

where $J_{2j-1}(z)$ is the $(2j-1)$-th Bessel function of the first kind. This represents the generation of the odd harmonics, $3\omega_{in}, 5\omega_{in}, 7\omega_{in}\cdots$ etc in addition to the original frequency ω_{in}. Relative to the fundamental, these harmonics will have amplitude

$$A_{(2j-1)\omega_{in}} = \frac{P_{sig,m_{sig}}P_{LO,m_{LO}}}{P_{sig,n_{sig}}P_{LO,n_{LO}}}\frac{J_{2j-1}\left(\frac{\pi A_{in}}{V_\pi}\right)}{J_1\left(\frac{\pi A_{in}}{V_\pi}\right)} \tag{24}$$

where n_{LO} and m_{LO} represent the channel (and therefore LO comb line) that the fundamental and $(2j-1)$-th harmonic respectively fall into, while n_{sig} and m_{sig} represents the signal comb lines that carry the fundamental and $(2j-1)$ th harmonic respectively, which may not equal the channel number if frequencies above $\omega_{sig}/2$ are generated. The formulae for calculating these indices are given by (41) and (42) in the Appendix.

These additional frequency components will propagate through the dual comb system as described for the linear case (7)-(12). Harmonic-harmonic and harmonic-fundamental beating (i.e. signal-signal beating) will be eliminated at the coherent receiver. We can therefore estimate the relative power of the harmonics to the fundamental by squaring and summing (24) to obtain the total harmonic distortion (THD)

$$\text{THD} = \left(\sum_{j=1}^{\infty} A^2_{(2j-1)\omega_{in}}\right)^{-1} \tag{25}$$

assuming that the strongest harmonic is for $j = 2$ (true unless significantly overdriving the modulator) we can also estimate the spurious free dynamic range (SFDR), which we can use as the SNR limit due to modulator nonlinearity

$$\text{SNR}_{mod} = \text{SFDR} = \frac{1}{A^2_{3\omega_{in}}} = \frac{P_{sig,n}P_{LO,n}}{P_{sig,m}P_{LO,m}}\frac{J_1\left(\frac{\pi A_{in}}{V_\pi}\right)^2}{J_3\left(\frac{\pi A_{in}}{V_\pi}\right)^2} \tag{26}$$

observing that SFDR $\approx$ THD. It is clear from the shape of the Bessel functions in (26) that minimising A_{in} is required to maximise SFDR. Strictly speaking, we should also modify the shot and thermal noise limits by accounting for reduction in signal power due to modulator nonlinearity. This can be done by the simple substitution

$$\frac{\pi A_{in}}{V_\pi} = J_1\left(\frac{\pi A_{in}}{V_\pi}\right). \tag{27}$$

For more complex input signals, additional inter-modulation distortion products are generated. We therefore also consider the case of a two tone input

$$V_{in}(t) = \frac{A_{in}}{\sqrt{2}}\sin(\omega_1 t) + \frac{A_{in}}{\sqrt{2}}\sin(\omega_2 t). \tag{28}$$

Considering only third order distortion products, this will result in additional frequencies at $3\omega_1, 3\omega_2, 2\omega_1-\omega_2, 2\omega_2-\omega_1, 2\omega_2+\omega_1, 2\omega_2-\omega_1$ whose amplitudes can be calculated by

Optics EXPRESS

considering the Taylor expansion of the modulator transfer function which is detailed in the Appendix. To determine the power of these products in the received signal, we multiply the square of the amplitudes by $4R^2P_{sig,m_{sig}}P_{LO,m_{LO}}$ where m_{sig}, m_{LO} are the calculated channel indices for the spurious tone, as calculated by (41) and (42). By comparing these noise powers to the received signal power, we can obtain the 3rd order intermodulation distortion (IMD3), and define SNR_{mod} = IMD3 for the two tone case. As per the single tone case, the shot/thermal noise equations should be modified to include the new amplitudes of the fundamental.

2.4. ADC noise

Phase noise induced sampling error and quantisation error will be introduced within each channel when the sub-band is digitised. The maximum SNR at each sub-ADC will be given by

$$\text{SNR}_{ADC} = \left[((\omega_{in} - n\Delta\omega)\sigma)^2 + \frac{1}{3 \cdot 2^{2K-1}}\right]^{-1} \tag{29}$$

for jitter σ where $\omega_{in} - n\Delta\omega < \frac{\Delta\omega}{2}$ and K the number of bits [41]. In a practical system, it will make more sense to simply determine the ADC SNR limit from its stated effective number of bits, while accounting for any SNR enhancement through oversampling within the sub-band.

3. Numerical simulation

To evaluate our theoretical estimates, we simulated single and two tone sine wave testing of an example channelizer. Two frequency combs were generated by modulating a seed laser via cascaded intensity and phase modulators as in [30]. External amplification might be used to boost the power of the seed source and result in additional spontaneous emission noise. However, one may use saturated amplifier to ensure high optical signal to noise ratio [11,42] such that the impact of spontaneous emission noise on the SINAD of the dual-comb channelizer is negligible. The laser phase noise is modelled as a Weiner process of linewidth 5 kHz. The comb driving sinusoids are generated with white phase noise across the uncorrelated jitter bandwidth (i.e. up to ± 500 MHz offset from carrier) using different seeds to a normally distributed Mersenne twister pseudorandom number generator. This bandlimited white phase noise represents the relative jitter after correlation and filtering effects are considered, as well as any decorrelation effects caused by path length mismatch. For reference, the optical power of each comb line is plotted in Fig. 8 in the Appendix.

The signal comb is modulated with the input RF signal, followed by demultiplex filtering and coherent detection of each modulated tone (sub-channel) as shown in Fig. 2. Blackman windowing functions are applied to the input test wave and each detected sub-channel in order

Table 1. Simulation parameters used for results presented in Fig. 4 and Fig. 5.

Parameter	Value	Parameter	Value
Number of samples	2^{24}	Seed laser power	37.5 dBm
Sample rate	2 THz	Number of channels, N	12
Signal comb spacing, f_{sig}	25 GHz	Demultiplex loss	4.8 dB
LO comb spacing, f_{LO}	26 GHz	Input modulator loss	3.4 dB
Sub-band bandwidth, Δf	1 GHz	Photodiode load resistance	10 kΩ
Total relative jitter, σ_j	9.47 fs	Laser linewidth	5 kHz
Comb insertion loss	7.4 dB	V_π	4 V
Photodiode responsivity	1.0 A/W	Temperature	300 K
ADC clock jitter	100 fs	ADC resolution	14 bits

Optics EXPRESS

to prevent spectral leakage. Photodiode thermal and shot noise are added at each sub-channel. Each detected sub-channel is then summed after being frequency shifted to its correct frequency band to reconstruct the complete input signal. Single tone SINAD and SFDR measurements are obtained by using a modified periodogram to estimate the power spectral density of the output signal, and comparing the relative power of the signal frequency bin to all others. For two tone testing, SINAD and IMD3 values are obtained by comparing the normalised output to the noiseless input signal. A complete list of simulation parameters can be found in Table 1.

4. Simulation and calculation results

Figure 4 shows the SINAD (Fig.4(a)) and the SFDR/IMD3 (Fig.4(b)) vs input frequency for an example 12-channel 12.5 GHz bandwidth channelizer, with 9.47 fs relative jitter. This jitter value is calculated from a line segment estimate to a commercially available oven controlled oscillator (OCXO) referenced microwave synthesizer, details of which are given in the Appendix. Plotted are SINAD, single tone SFDR, and two tone IMD3 estimates from the simulation described in the previous section and theoretical estimates derived by summing the derived expressions for photodiode noise, ADC noise, modulator nonlinearity and phase noise. The two tone IMD3 estimate is determined by an input signal equal in power to the single tone case with input frequencies f_{in}, f_{in} + 100 MHz. Also plotted are the photodiode shot noise (green solid line), photodiode thermal noise (orange solid line) phase noise limited SINAD (black solid line) to illustrate the limits imposed by the main stochastic noise processes, along with the sub-band ADC SINAD limit (solid blue line) which has neglitible impact on the overall SINAD even at a modest ADC clock jitter (100 fs).

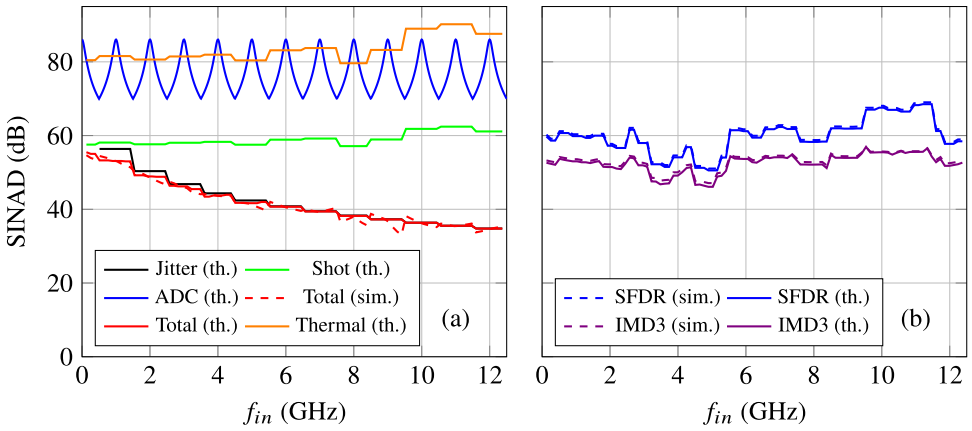

Fig. 4. Input test signal frequency f_{in} vs (a) SINAD and (b) SFDR/IMD3 for a 12 channel 12.5 GHz bandwidth jitter limited channelizer based on dual combs generated by cascaded intensity and phase modulator, with 9.47 fs relative jitter. IMD3 measurements (b) are obtained from the equivalent power two tone input signal, where the second tone is +100 MHz from f_{in}. The shot noise, jitter limited and ADC limited SINAD are also shown. Sim., numerical simulation results; th., theoretical calculation from our models.

As shown in Fig. 4(a), the SINAD of the channelizer is limited by the relative jitter, and essentially follows the jitter limit except for low frequencies, where shot noise and nonlinearity become prominent. The SINAD/SFDR/IMD3 plots show broad agreement between the simulation (dashed lines) and theoretical (solid lines) estimates. The shot noise limit follows the power variation between the comb lines (see Fig. 8 in the Appendix), showing the 'bat ears' shape that is characteristic of the cascaded phase and intensity modulator comb generating method [30]. Both SFDR and IMD3 are more strongly affected by this variation in comb line power and see

Optics EXPRESS

strong fluctuations (up to 20 dB) across the input bandwidth. This is because the SFDR/IMD3 for a given input frequency is dependent on the relative strength of the fundamental and generated harmonics, so will increased dramatically if the harmonics fall into a low power channel and the fundamental into a high power channel, and drop dramatically if the reverse is true. We can see from Fig. 4(b) therefore even the small variations in frequency comb power in this case (see Fig. 8) can lead to strong variations in SFDR/IMD3, which highlights the importance of generating a flat frequency comb if minimizing these fluctuations is important for the application.

Figure 5 shows SINAD and harmonic distortion for a low relative jitter ($\approx$ 1 fs) scenario as a function of the A_{in}/V_{π}, with Fig. 5(a) showing a single tone input of 2.2 GHz and with Fig. 5(b) showing the equivalent power two tone case at 2.2 GHz and 2.3 GHz. When the relative jitter is sufficiently low, the limiting factors for SINAD become SFDR/IMD3 and shot noise. This is typical of any analog optical link: driving the modulator with a low A_{in} gives a low harmonic distortion but results in a high level of shot noise, and vice versa. Thus there exists some peak value of SINAD where the penalties from nonlinearity and shot noise are balanced, as seen at around $A_{in}/V_{\pi} = 0.045$ in Fig. 5(a) and $A_{in}/V_{\pi} = 0.035$ in Fig. 5(b).

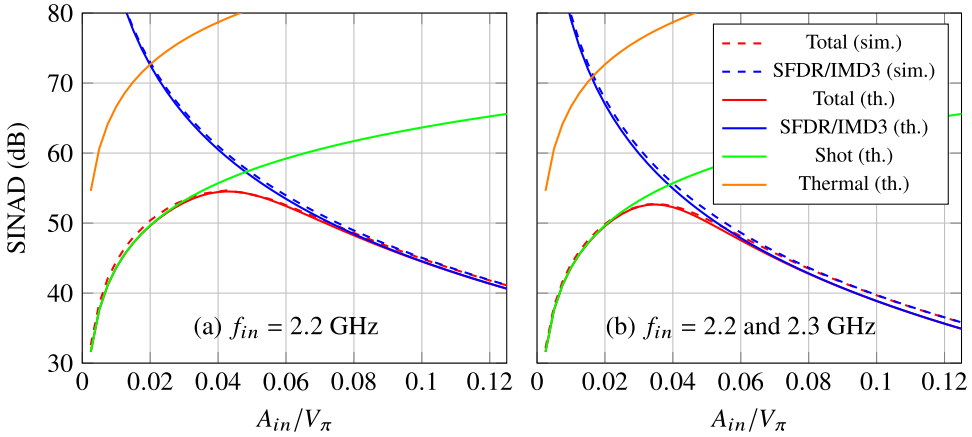

Fig. 5. A_{in}/V_{π} v SINAD for shot noise/harmonic distortion limited 12 channel 12.5 GHz channelizer. (a) shows single tone SINAD/SFDR at 2.2 GHz, (b) shows two tone SINAD/IMD3 with 2.2 and 2.3 GHz inputs. Sim., numerical simulation results; th., theoretical calculation from our models.

Since the modulation transfer function is known, analog or digital compensation functions can be applied that attempt to reverse the distortion introduced by the modulator and effectively shift the peak SINAD value to higher A_{in}/V_{π} values in Fig. 5. Digital techniques operating at gigasample rates have been demonstrated that achieved up to 30 dB suppression of the third order harmonic [26,27], and analog techniques achieving as much as 45 dB suppression [28]. Clearly, the increased level of harmonic distortion in Fig. 5(b) due to the presence of additional inter-modulation distortion products shows that this linearization is increasingly important for more complex input signals.

The simulation (dashed lines) and theoretical estimates (solid lines) for SINAD and SFDR are in close agreement. Note that the thermal noise limit is well above the shot noise floor in this case due to the high photodiode load (10k Ω), but thermal noise will begin to contribute if the photodiode load is low or the optical power is low. If thermal noise does become a factor, it exhibits a tradeoff with harmonic distortion in the same way as shot noise.

Optics EXPRESS

5. Discussion and performance limits

After confirming the theoretical modelling with numerical simulation, we expand our discussion to general dual comb systems which may use different comb techniques or target a different bandwidth, and therefore have different number of channels and optical power. Figure 6(a) shows how the worst case SINAD (i.e. for the N-th, or highest, channel) changes with total comb power (assuming the same power for each tone) for a variety of channelizer configurations at 25 GHz bandwidth and is illustrative of the general performance trends for dual frequency comb channelizers. The jitter values are full bandwidth jitter values that assume that the uncorrelated jitter has a white spectrum, and therefore scales with $1/\sqrt{N}$. A relative jitter of 50 fs represents that achievable between two electro-optic frequency combs referenced to a typical high quality commercial oscillator. On the other hand, 1 fs represents jitter levels for state of the photonic approaches, where the frequency comb is referenced to a high quality optical reference cavity [43–45].

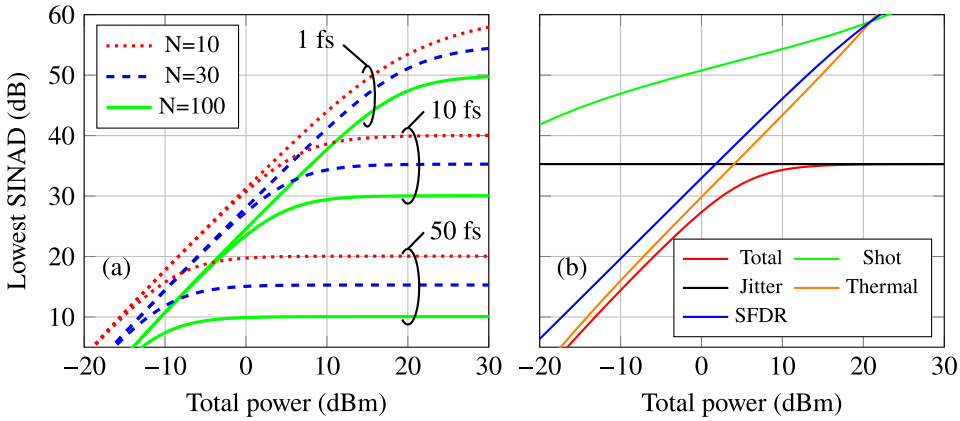

Fig. 6. Lowest SINAD (i.e. the N-th channel) as a function of total comb power for a 25 GHz channelizer, with A_{in} optimised to minimise the total noise contribution from shot noise, thermal noise and SFDR. (a) shows a variety of channel numbers, N, and relative jitters, while (b) shows the constituent noise contributions for the N = 10, jitter = 10 fs case. The photodiode load is assumed to be 50 Ω, demultiplex loss is 3 dB and modulator insertion loss is 3.4 dB.

Generally, increasing the total comb power will increase SINAD until it saturates at certain level due to the phase noise contribution, which is independent of power. This is seen more clearly in Fig. 6(b) which separates out the constituent noise components for the N = 30, jitter = 10 fs case. At low powers, thermal noise and SFDR is the dominant noise contribution until the relative jitter caps the SINAD at approximately 35 dB. The effect of changing the number of channels is seen in Fig. 6(a): more channels leads to lower total SINAD in all cases, since it increases shot and thermal noise due to less power per comb line and phase noise due to the highest channel being detected further from the frequency comb centre. This penalty may be outweighed however by the advantages of lower bandwidth analog and digital signal processing in the narrower channels.

This is further seen in Fig. 7, which shows the worst case SINAD as a function of total channelizer bandwidth, assuming a fixed total comb power of 10 dBm. Here there is also a consistent penalty with increasing N across all scenarios in Fig. 7(a), and the different relative jitters converge at low bandwidths where the thermal/shot noise and SFDR become the limiting noise factors. At high bandwidths phase noise limits the achievable SINAD as is clearly seen in Fig. 7(b), which plots the separate noise components for the N = 30, jitter = 10 fs case. Note that

Optics EXPRESS

achieving these theoretical limits in a low bandwidth (<10 GHz) channelizer may be challenging due to the narrow optical filtering required, which although achievable for example via optical injection locking [46,47], can introduce additional absolute phase noise or decorrelation.

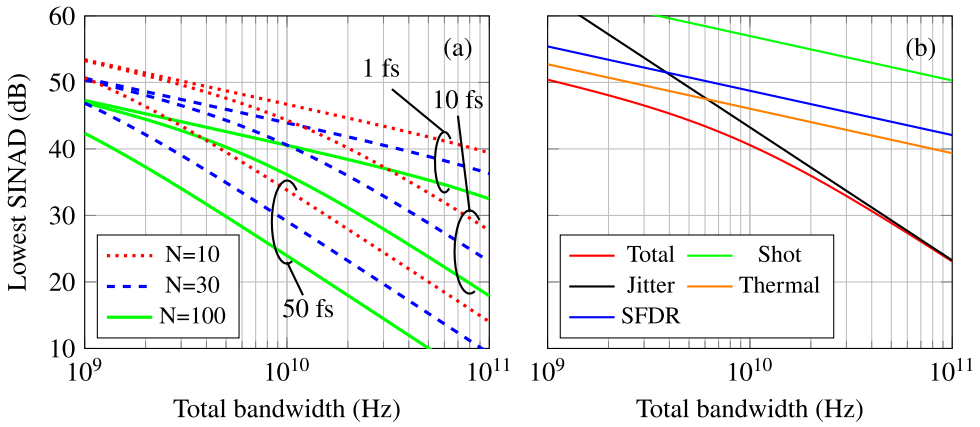

Fig. 7. Lowest SINAD (i.e. the N-th channel) as a function of total channelizer bandwidth for a total comb power of 10 dBm, with A_{in} optimised to minimise the total noise contribution from shot noise, thermal noise and SFDR. (a) shows a variety of channel numbers, N, and relative jitters, while (b) shows the constituent noise contributions for the $N = 30$, jitter = 10 fs case. The photodiode load is assumed to be 50 Ω., demultiplex loss is 3 dB and modulator insertion loss is 3.4 dB.

Both graphs highlight the dual comb channelizer's extreme sensitivity to relative phase noise when trying to achieve high accuracy and bandwidth. Indeed, Fig. 6(a) and Fig. 7(a) display how a relative jitter of only 50 fs will result in a phase noise limited channelizer in most cases. This may not be a problem in high noise and spread spectrum applications such as [8–10], but emphasises the importance of broadband phase noise correlation between the comb sources or low absolute jitter if high SINAD is required. Furthermore, the phase noise correlation between comb lines [48] may allow for novel digital signal processing schemes that can efficiently compensate the phase noise discussed here to some degree [49–51].

Finally, it is important to emphasize that the fundamental performance parameters discussed in this paper are not the only factors that will determine the extent to which dual frequency combs can be used as channelizers. The practical implementation of the dual-comb channelizer would benefit from the rapid development of photonic integrated circuits, which allow for high performance frequency comb sources, minimized channel mismatch and high density coherent receiver arrays that drives down the cost and power consumption. Heterogeneous integration that harnesses the benefit of different integration platforms, including silicon nitride [17,18,52] and thin lithium niobate [53–56] and high performance III-V/Si/Si_3N_4 on silicon light sources [57,58], could lead to a promising integrated solution for the dual-comb channelizer.

6. Conclusion

This paper has detailed a theoretical analysis of high bandwidth dual frequency comb channelizers for RF signal processing to assess which factors limit the achievable signal to noise and distortion ratio. Our theoretical estimates were tested against a simulation model in an example performance analysis, which demonstrated how the noise contributions varied across the channelizer bandwidth and how the signal driving power affects the observed SINAD. In a broader discussion of dual comb channelizers, we showed that while sufficient comb power is important for overcoming

Optics EXPRESS

thermal and shot noise limits, the dual comb channelizer is ultimately sensitive to the relative phase noise between the two frequency combs in high bandwidth scenarios.

7. Appendix

7.1. Frequency comb power for Section 3

Figure 8 shows the optical power of the frequency combs used in the simulation in Section 3 as a function of the line number.

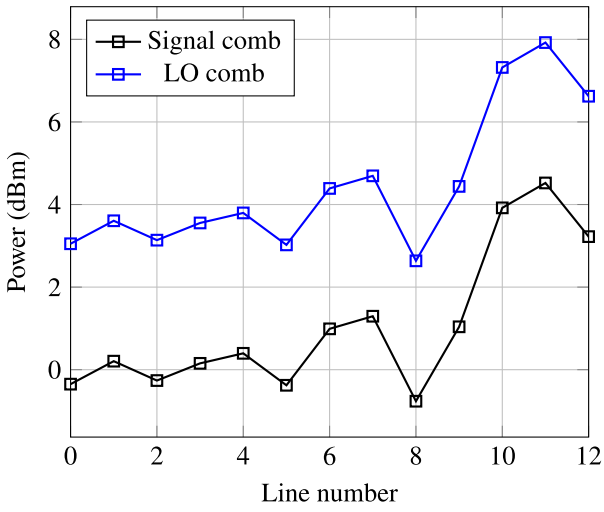

Fig. 8. Optical power vs frequency comb line number for the frequency combs generated in the simulation described in Section 3.

7.2. Relative jitter estimation for Section 3

In order to obtain a reasonable estimate for relative jitter we show in Fig. 9 a line segment approximation for a commerically available microwave synthesiser (Rohde and Schwarz SMAB-B711(N)) operating at 20 GHz. Scaling these phase noise levels by $(25/20)^2$ and $(26/20)^2$ gives us an estimate of the phase noise level for 25 GHz and 26 GHz respectively. The data sheet suggests that the internal loop filter is around 1 kHz: phase noise between two synthesizers below this frequency will be correlated and above it uncorrelated.

We can now plug these estimates into (18)

$$S_{\Delta\phi_n}(\omega) = n^2\left[\left|\frac{26-25}{20}\right|^2|\phi_c(\omega)|^2 + \left|\frac{26}{20}\phi_{u,LO}(\omega)\right|^2 + \left|\frac{25}{20}\phi_{u,sig}(\omega)\right|^2\right] \tag{30}$$

and calculate the phase noise power in dBc using (14), writing the spectrum in Fig. 9 as $|\phi_{RS}(\omega)|^2$

$$\frac{\overline{\Delta\phi_n^2}}{2n^2} = \frac{1}{20^2}\int_{10\text{ Hz}}^{1\text{ kHz}}|\phi_{RS}(f)|^2\mathrm{d}f + \left[\left(\frac{26}{20}\right)^2 + \left(\frac{25}{20}\right)^2\right]\int_{1\text{ kHz}}^{500\text{ MHz}}|\phi_{RS}(f)|^2\mathrm{d}f \tag{31}$$

$$= 3.43\times10^{-10} + 4.83\times10^{-7} + 4.46\times10^{-7} \tag{32}$$

$$\overline{\Delta\phi_n^2} = n^2(1.86\times10^{-6}) \tag{33}$$

Optics EXPRESS

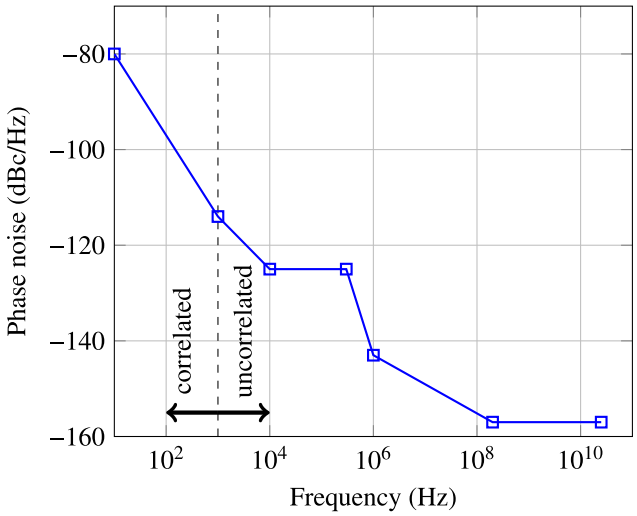

Fig. 9. Phase noise spectrum used for the example analysis in this paper: this is a line segment approximation for the Rohde and Schwarz SMAB-B711(N) at 20 GHz. Note that by convention this is single sided phase noise spectral density, $\mathcal{L}(f) = S_\phi(f)/2$.

noting the limits defined by our loop bandwidth estimate and sub-channel bandwidth, $\frac{\Delta f}{2} = 500$ MHz. In terms of relative jitter (19) this is

$$\sigma_j = \sqrt{\frac{2 \times 3.43 \times 10^{-10}}{(2\pi \times 1\ \text{GHz})^2} + \frac{2 \times 4.83 \times 10^{-7}}{(2\pi \times 25\ \text{GHz})^2} + \frac{2 \times 4.46 \times 10^{-7}}{(2\pi \times 26\ \text{GHz})^2}} = 9.47\ \text{fs} \tag{34}$$

which corresponds to 6.70 fs uncorrelated contribution from each comb.

7.3. Arbitrary input signal

Our phase noise analysis from (8)-(12) can be extended to any arbitrary input up to the channelizer bandwidth, by representing the input signal as the sum of its Fourier components

$$V_{in}(t) = \frac{a_0}{2} + \sum_{p=1}^{P} (a_p \cos(\omega p t) + b_p \sin(\omega p t)) \tag{35}$$

given that the duration $2\pi/\omega$ is finite and that $P < \frac{\omega_{sig}}{2\omega}$. Each channel will detect a sub-band of the input signal so it is simpler to split the input signal into each sub-band

$$V_{in}(t) = \frac{a_0}{2} + \sum_{n=0}^{N} \sum_{p=(n-\frac{1}{2})\frac{\Delta\omega}{\omega}}^{(n+\frac{1}{2})\frac{\Delta\omega}{\omega}} (a_p \cos(\omega p t) + b_p \sin(\omega p t)) \tag{36}$$

and the photodiode noise Eqs. (21)/(22) can be modified by replacing of the mean power the sine wave, $\frac{A_{in}^2}{2}$, with

$$\frac{A_{in}^2}{2} = \sum_{p=(n-\frac{1}{2})\frac{\Delta\omega}{\omega}}^{(n+\frac{1}{2})\frac{\Delta\omega}{\omega}} \left[\frac{a_p^2}{2} + \frac{b_p^2}{2}\right] \tag{37}$$

which is simply the signal power within each sub-channel.

Optics EXPRESS

7.4. Third order harmonic distortion products amplitudes

For a two tone input

$$V_{in}(t) = A_1 \sin(\omega_1 t) + A_2 \sin(\omega_2 t) \tag{38}$$

the modulator transfer function has output

$$M(V_{in}(t)) = \sin\left[\frac{\pi}{V_\pi}(A_1 \sin(\omega_1 t) + A_2 \sin(\omega_2 t))\right] \tag{39}$$

$$= \frac{\pi}{V_\pi}(A_1 \sin(\omega_1 t) + A_2 \sin(\omega_2 t)) - \frac{1}{3!}\left(\frac{\pi}{V_\pi}\right)^3 (A_1 \sin(\omega_1 t) + A_2 \sin(\omega_2 t))^3 + \cdots \tag{40}$$

considering the first two terms of the sine expansion (i.e. up to cubic order) gives the so-called third order harmonics, whose amplitudes are given in Table 2.

Table 2. Third order harmonic distortion products amplitudes.

Frequency	Amplitude	Frequency	Amplitude
ω_1	$\frac{\pi A_1}{V_\pi} - \frac{1}{24}\left(\frac{\pi}{V_\pi}\right)^3 (3A_1^3 + 6A_1A_2^2)$	ω_2	$\frac{\pi A_2}{V_\pi} - \frac{1}{24}\left(\frac{\pi}{V_\pi}\right)^3 (3A_2^3 + 6A_2A_1^2)$
$2\omega_1 - \omega_2$	$\frac{1}{8}\left(\frac{\pi}{V_\pi}\right)^3 A_1^2 A_2$	$2\omega_2 - \omega_1$	$\frac{1}{8}\left(\frac{\pi}{V_\pi}\right)^3 A_2^2 A_1$
$2\omega_1 + \omega_2$	$\frac{1}{8}\left(\frac{\pi}{V_\pi}\right)^3 A_1^2 A_2$	$2\omega_2 + \omega_1$	$\frac{1}{8}\left(\frac{\pi}{V_\pi}\right)^3 A_2^2 A_1$
$3\omega_1$	$\frac{1}{24}\left(\frac{\pi A_1}{V_\pi}\right)^3$	$3\omega_2$	$\frac{1}{24}\left(\frac{\pi A_2}{V_\pi}\right)^3$

7.5. Channel number (comb line indices) for a given input frequency

For a dual comb system with signal comb frequency ω_{sig} and spacing $\Delta\omega$, the frequency ω (whether the desired input or subsequently generated harmonic), will fall into channel

$$m_{LO} = \left\lceil \frac{\left|\omega - \omega_{sig}\left\lceil \frac{\omega}{\omega_{sig}} \right\rceil\right|}{\Delta\omega} \right\rceil \tag{41}$$

where $\lceil x \rceil$ denotes rounding x to the nearest integer, where half is rounded up. This means that it will be detected by the m_{LO}-th LO comb line, and will be carried by the m_{sig}-th signal comb line, given by

$$m_{sig} = \left| n_{LO} + (-1)^{\left\lceil \frac{\omega}{2\omega_{sig}} \right\rceil} \left\lceil \frac{\omega}{\omega_{sig}} \right\rceil \right|. \tag{42}$$

Note that for $\omega < \frac{\omega_{sig}}{2}$ this reduces to

$$m_{sig} = m_{LO} = \left\lceil \frac{\omega}{\Delta\omega} \right\rceil. \tag{43}$$

7.6. Optical path length mismatch

Consider that one of the optical paths in the dual comb arrangement is mismatched from the other by length ΔL, corresponding to a time delay of $\Delta T = \Delta L \frac{n_{\text{eff}}}{c}$, for a refractive index of n_{eff}. This means that the laser phase noise (often defined by its linewidth) on each path, in both the time and frequency domain, will be

$$\phi_0(t) \overset{\text{FT}}{\Rightarrow} \phi_0(\omega) \tag{44}$$

$$\phi_0(t + \Delta T) \overset{\text{FT}}{\Rightarrow} e^{i\omega\Delta T}\phi_0(\omega) \tag{45}$$

instead of perfect cancellation at the coherent receiver as assumed earlier, each branch will experience a time delay (phase rotation) that decorrelates the phase noise between the two

Optics EXPRESS

branches and converts it to intensity noise at the coherent receiver. The amount of phase rotation is dependent on the offset frequency and ΔT. At a specific offset frequency $f = 2\pi\omega$ we can consider the power of the residual laser phase noise observed at the coherent receiver due to the length mismatch

$$|\phi_0(\omega) - e^{i\omega\Delta T}\phi_0(\omega)|^2 = |1 - e^{i\omega\Delta T}|^2|\phi_0(\omega)|^2 \tag{46}$$

plotting

$$|1 - e^{i\omega\Delta T}|^2 = 2 - 2\cos(\omega\Delta T) \tag{47}$$

shows us therefore the laser phase noise suppression at the coherent receiver in Fig. 10(a). This laser phase noise suppression can be applied to the power spectral density of the laser phase noise to determine the phase noise power spectral density at the coherent receiver caused by the laser phase noise. To illustrate this, we can use the common approximation that the laser phase noise single sided power spectral density follows a random walk [59]

$$S_{\text{laser}}(f) = \frac{\delta\nu}{\pi f^2} \tag{48}$$

where $\delta\nu$ is the laser linewidth. Multiplying (48) by the suppression factor (47) will result in a white phase noise at the coherent receiver, which is plotted in Fig. 10(b) versus linewidth for a variety of length mismatches. Even for a 1 mm mismatch at 5 kHz linewidth, the laser phase noise level is at -178 dBc/Hz, implying a SINAD limit of 88 dB across for example 1 GHz bandwidth, well above the SINAD of the other effects described in the paper. Furthermore, any time-dependent optical path length mismatches induced by temperature and mechanical vibrations can be minimised by using an integrated platform or using active phase stability techniques [60,61].

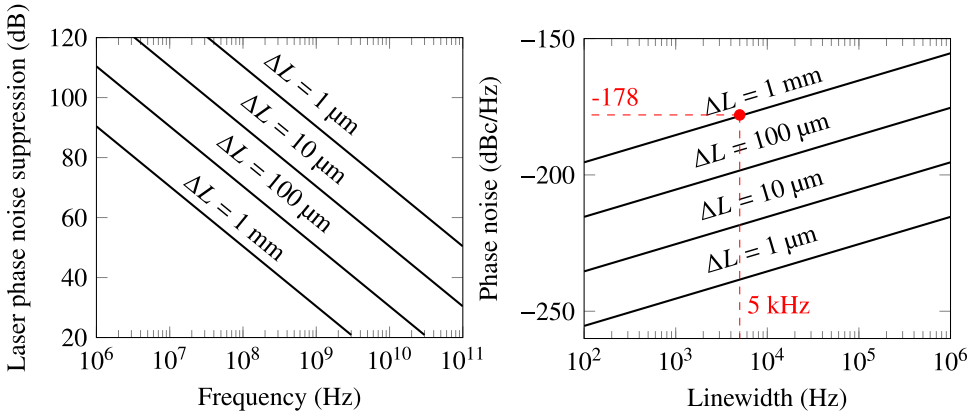

Fig. 10. (a) Laser phase noise suppression (47) as a function of offset frequency, for $n_{\text{eff}} = 1.44$. (b) Residual laser phase noise at the coherent receiver as a function of laser linewidth assuming a random walk. A 5 kHz linewidth example giving -178 dBc/Hz at 1 mm length mismatch is labelled in red.

Funding

Royal Society (PIF/R1/180001); Engineering and Physical Sciences Research Council (EP/R035342/1, EP/R041792/1, EP/R512400/1).

Acknowledgements

The authors thank Prof. Enrico Rubiola and Prof. Paul Brennan for helpful discussions. Callum Deakin acknowledges the support of an AHW Beck Memorial Scholarship.

Optics EXPRESS

Disclosures

The authors declare no conflict of interests.

References

1. M. S. Alshaykh, J. D. McKinney, and A. M. Weiner, "Radio-frequency signal processing using optical frequency combs," IEEE Photonics Technol. Lett. **31**(23), 1874–1877 (2019).
2. I. Coddington, N. Newbury, and W. Swann, "Dual-comb spectroscopy," Optica **3**(4), 414 (2016).
3. S. Schiller, "Spectrometry with frequency combs," Opt. Lett. **27**(9), 766–768 (2002).
4. N. R. Newbury, I. Coddington, and W. Swann, "Sensitivity of coherent dual-comb spectroscopy," Opt. Express **18**(8), 7929–7945 (2010).
5. X. Xie, Y. Dai, K. Xu, J. Niu, R. Wang, L. Yan, and J. Lin, "Broadband photonic RF channelization based on coherent optical frequency combs and I/Q demodulators," IEEE Photonics J. **4**(4), 1196–1202 (2012).
6. A. Wiberg, D. Esman, L. Liu, J. Adleman, S. Zlatanovic, V. Ataie, E. Myslivets, B. P.-P. Kuo, N. Alic, E. Jacobs, and S. Radic, "Coherent filterless wideband microwave/millimeter-wave channelizer based on broadband parametric mixers," J. Lightwave Technol. **32**(20), 3609–3617 (2014).
7. A. Klee, C. Middleton, and R. DeSalvo, "Dual-comb spectrometer for fast wideband RF spectral analysis," in *2017 IEEE Photonics Conference (IPC)*, (IEEE, 2017), p. WA1.1.
8. V. Ataie, D. Esman, B. P.-P. Kuo, N. Alic, and S. Radic, "Subnoise detection of a fast random event," Science **350**(6266), 1343–1346 (2015).
9. D. J. Esman, V. Ataie, B. P. Kuo, E. Temprana, N. Alic, and S. Radic, "Detection of Fast Transient Events in a Noisy Background," J. Lightwave Technol. **34**(24), 5669–5674 (2016).
10. H. Hu, V. Ataie, E. Myslivets, and S. Radic, "Optical comb assisted OFDM RF receiver," J. Lightwave Technol. **37**(4), 1280–1287 (2019).
11. C. Deakin and Z. Liu, "Dual frequency comb assisted analog-to-digital conversion," Opt. Lett. **45**(1), 173–176 (2020).
12. C. Deakin, T. Odedeyi, and Z. Liu, "Dual frequency comb photonic analog to digital conversion," in *2020 IEEE Photonics Society Summer Topicals Meeting Series (SUM)*, (IEEE, 2020), p. WB4.3.
13. A. Lukashchuk, J. Riemensberger, J. Liu, P. Marin-Palomo, M. Karpov, C. Koos, R. Bouchand, and T. J. Kippenberg, "Photonic-assisted analog-to-digital conversion using integrated soliton microcombs," in *45th European Conference on Optical Communication (ECOC 2019)*, (2019), p. Th.2.E.6.
14. M. S. Alshaykh, D. E. Leaird, J. D. McKinney, and A. M. Weiner, "Rapid wideband RF subsampling and disambiguation using dual combs," in *CLEO: Science and Innovations*, (Optical Society of America, 2019), p. SF2N.8.
15. B. Liu, A. Shakouri, and J. E. Bowers, "Wide tunable double ring resonator coupled lasers," IEEE Photonics Technol. Lett. **14**(5), 600–602 (2002).
16. T. Claes, W. Bogaerts, and P. Bienstman, "Experimental characterization of a silicon photonic biosensor consisting of two cascaded ring resonators based on the Vernier-effect and introduction of a curve fitting method for an improved detection limit," Opt. Express **18**(22), 22747–22761 (2010).
17. P. Del'Haye, A. Schliesser, O. Arcizet, T. Wilken, R. Holzwarth, and T. J. Kippenberg, "Optical frequency comb generation from a monolithic microresonator," Nature **450**(7173), 1214–1217 (2007).
18. Y. Okawachi, K. Saha, J. S. Levy, Y. H. Wen, M. Lipson, and A. L. Gaeta, "Octave-spanning frequency comb generation in a silicon nitride chip," Opt. Lett. **36**(17), 3398–3400 (2011).
19. E. Myslivets, B. P. Kuo, N. Alic, and S. Radic, "Generation of wideband frequency combs by continuous-wave seeding of multistage mixers with synthesized dispersion," Opt. Express **20**(3), 3331–3344 (2012).
20. E. Rubiola, *Phase noise and frequency stability in oscillators* (Cambridge University Press, 2009).
21. C. W. Nelson, A. Hati, and D. A. Howe, "Relative intensity noise suppression for RF photonic links," IEEE Photonics Technol. Lett. **20**(18), 1542–1544 (2008).
22. D. Kim, S. Zhang, D. Kwon, R. Liao, Y. Cui, Z. Zhang, Y. Song, and J. Kim, "Intensity noise suppression in mode-locked fiber lasers by double optical bandpass filtering," Opt. Lett. **42**(20), 4095–4098 (2017).
23. X. Xie, J. Khurgin, J. Kang, and F.-S. Chow, "Linearized Mach-Zehnder intensity modulator," IEEE Photonics Technol. Lett. **15**(4), 531–533 (2003).
24. H. Yamazaki, H. Takahashi, T. Goh, Y. Hashizume, T. Yamada, S. Mino, H. Kawakami, and Y. Miyamoto, "Optical modulator with a near-linear field response," J. Lightwave Technol. **34**(16), 3796–3802 (2016).
25. A. Khilo, C. M. Sorace, and F. X. Kärtner, "Broadband linearized silicon modulator," Opt. Express **19**(5), 4485–4500 (2011).
26. T. Clark, M. Currie, and P. Matthews, "Digitally linearized wide-band photonic link," J. Lightwave Technol. **19**(2), 172–179 (2001).
27. Y. Cui, Y. Dai, F. Yin, Q. Lv, J. Li, K. Xu, and J. Lin, "Enhanced spurious-free dynamic range in intensity-modulated analog photonic link using digital postprocessing," IEEE Photonics J. **6**(2), 1–8 (2014).
28. W. Jiang, Q. Tan, W. Qin, D. Liang, X. Li, H. Ma, and Z. Zhu, "A linearization analog photonic link with high third-order intermodulation distortion suppression based on dual-parallel Mach-Zehnder modulator," IEEE Photonics J. **7**(3), 1–8 (2015).

Optics EXPRESS

29. R. H. Walden, "Analog-to-digital conversion in the early twenty-first century," *Wiley Encyclopedia of Computer Science and Engineering* pp. 1–14 (2007).
30. V. Torres-Company, J. Lancis, and P. Andrés, "Lossless equalization of frequency combs," Opt. Lett. **33**(16), 1822–1824 (2008).
31. A. Ishizawa, T. Nishikawa, A. Mizutori, H. Takara, A. Takada, T. Sogawa, and M. Koga, "Phase-noise characteristics of a 25-GHz-spaced optical frequency comb based on a phase-and intensity-modulated laser," Opt. Express **21**(24), 29186–29194 (2013).
32. K. Nishimoto, K. Minoshima, T. Yasui, and N. Kuse, "Investigation of the phase noise of a microresonator soliton comb," Opt. Express **28**(13), 19295–19303 (2020).
33. "IEEE standard definitions of physical quantities for fundamental frequency and time metrology—random instabilities," *IEEE Std Std 1139-2008* pp. c1–35 (2009).
34. B. Brannon, "Sampled systems and the effects of clock phase noise and jitter," *Analog Devices App. Note AN-756* pp. 1–11 (2004).
35. D. Rönnow, S. Amin, M. Alizadeh, and E. Zenteno, "Phase noise coherence of two continuous wave radio frequency signals of different frequency," IET Sci. Meas. & Technol. **11**(1), 77–85 (2017).
36. Z. Tong, A. O. Wiberg, E. Myslivets, B. P. Kuo, N. Alic, and S. Radic, "Spectral linewidth preservation in parametric frequency combs seeded by dual pumps," Opt. Express **20**(16), 17610–17619 (2012).
37. A. B. Matsko, A. A. Savchenkov, N. Yu, and L. Maleki, "Whispering-gallery-mode resonators as frequency references. I. Fundamental limitations," J. Opt. Soc. Am. B **24**(6), 1324–1335 (2007).
38. W. Liang, D. Eliyahu, V. S. Ilchenko, A. A. Savchenkov, A. B. Matsko, D. Seidel, and L. Maleki, "High spectral purity Kerr frequency comb radio frequency photonic oscillator," Nat. Commun. **6**(1), 7957–7958 (2015).
39. A. B. Matsko and L. Maleki, "Noise conversion in Kerr comb RF photonic oscillators," J. Opt. Soc. Am. B **32**(2), 232–240 (2015).
40. K. Kikuchi and S. Tsukamoto, "Evaluation of sensitivity of the digital coherent receiver," J. Lightwave Technol. **26**(13), 1817–1822 (2008).
41. R. H. Walden, "Analog-to-digital converter survey and analysis," IEEE J. Select. Areas Commun. **17**(4), 539–550 (1999).
42. A. W. S. Putra, M. Yamada, H. Tsuda, and S. Ambran, "Theoretical analysis of noise in erbium doped fiber amplifier," IEEE J. Quantum Electron. **53**(4), 1–8 (2017).
43. T. M. Fortier, C. W. Nelson, A. Hati, F. Quinlan, J. Taylor, H. Jiang, C. Chou, T. Rosenband, N. Lemke, A. Ludlow, D. Howe, C. W. Oates, and S. A. Diddams, "Sub-femtosecond absolute timing jitter with a 10 GHz hybrid photonic-microwave oscillator," Appl. Phys. Lett. **100**(23), 231111 (2012).
44. D. R. Carlson, D. D. Hickstein, W. Zhang, A. J. Metcalf, F. Quinlan, S. A. Diddams, and S. B. Papp, "Ultrafast electro-optic light with subcycle control," Science **361**(6409), 1358–1363 (2018).
45. K. Beha, D. C. Cole, P. Del'Haye, A. Coillet, S. A. Diddams, and S. B. Papp, "Electronic synthesis of light," Optica **4**(4), 406–411 (2017).
46. D. S. Wu, D. J. Richardson, and R. Slavík, "Optical Fourier synthesis of high-repetition-rate pulses," Optica **2**(1), 18–26 (2015).
47. Z. Liu and R. Slavík, "Optical injection locking: From principle to applications," J. Lightwave Technol. **38**(1), 43–59 (2020).
48. L. Lundberg, M. Mazur, A. Fiilöp, V. Torres-Company, M. Karlsson, and P. A. Andrekson, "Phase correlation between lines of electro-optical frequency combs," in *CLEO: Science and Innovations*, (Optical Society of America, 2018), p. JW2A.149.
49. L. Lundberg, M. Mazur, A. Mirani, B. Foo, J. Schröder, V. Torres-Company, M. Karlsson, and P. A. Andrekson, "Phase-coherent lightwave communications with frequency combs," Nat. Commun. **11**(1), 201 (2020).
50. L. Lundberg, M. Mazur, A. Lorences-Riesgo, M. Karlsson, and P. A. Andrekson, "Joint carrier recovery for DSP complexity reduction in frequency comb-based superchannel transceivers," in *2017 European Conference on Optical Communication (ECOC)*, (2017), p. Th.1.D.3.
51. L. Lundberg, M. Karlsson, A. Lorences-Riesgo, M. Mazur, J. Schröder, and P. A. Andrekson, "Frequency comb-based wdm transmission systems enabling joint signal processing," Appl. Sci. **8**(5), 718 (2018).
52. C. G. Roeloffzen, L. Zhuang, C. Taddei, A. Leinse, R. G. Heideman, P. W. van Dijk, R. M. Oldenbeuving, D. A. Marpaung, M. Burla, and K.-J. Boller, "Silicon nitride microwave photonic circuits," Opt. Express **21**(19), 22937–22961 (2013).
53. C. Wang, M. Zhang, M. Yu, R. Zhu, H. Hu, and M. Loncar, "Monolithic lithium niobate photonic circuits for Kerr frequency comb generation and modulation," Nat. Commun. **10**(1), 1–6 (2019).
54. M. Zhang, B. Buscaino, C. Wang, A. Shams-Ansari, C. Reimer, R. Zhu, J. M. Kahn, and M. Lončar, "Broadband electro-optic frequency comb generation in a lithium niobate microring resonator," Nature **568**(7752), 373–377 (2019).
55. M. He, M. Xu, Y. Ren, J. Jian, Z. Ruan, Y. Xu, S. Gao, S. Sun, X. Wen, L. Zhou, L. Liu, C. Guo, H. Chen, S. Yu, L. Liu, and X. Cai, "High-performance hybrid silicon and lithium niobate Mach-Zehnder modulators for 100 Gbit s^{-1} and beyond," Nat. Photonics **13**(5), 359–364 (2019).
56. P. O. Weigel, J. Zhao, K. Fang, H. Al-Rubaye, D. Trotter, D. Hood, J. Mudrick, C. Dallo, A. T. Pomerene, A. L. Starbuck, C. T. DeRose, A. L. Lentine, G. Rebeiz, and S. Mookherjea, "Bonded thin film lithium niobate modulator

Optics EXPRESS

on a silicon photonics platform exceeding 100 GHz 3-dB electrical modulation bandwidth," Opt. Express **26**(18), 23728–23739 (2018).
57. C. Xiang, W. Jin, J. Guo, J. D. Peters, M. Kennedy, J. Selvidge, P. A. Morton, and J. E. Bowers, "Narrow-linewidth III-V/Si/Si_3N_4 laser using multilayer heterogeneous integration," Optica **7**(1), 20–21 (2020).
58. S. Gundavarapu, G. M. Brodnik, M. Puckett, T. Huffman, D. Bose, R. Behunin, J. Wu, T. Qiu, C. Pinho, N. Chauhan, J. Nohava, P. T. Rakich, K. D. Nelson, M. Salit, and D. J. Blumenthal, "Sub-hertz fundamental linewidth photonic integrated Brillouin laser," Nat. Photonics **13**(1), 60–67 (2019).
59. S. Camatel and V. Ferrero, "Narrow linewidth CW laser phase noise characterization methods for coherent transmission system applications," J. Lightwave Technol. **26**(17), 3048–3055 (2008).
60. Z. Liu, J. Kakande, B. Kelly, J. O'Carroll, R. Phelan, D. J. Richardson, and R. Slavík, "Modulator-free quadrature amplitude modulation signal synthesis," Nat. Commun. **5**(1), 5911–5917 (2014).
61. Z. Chen, M. Yan, T. W. Hänsch, and N. Picqué, "A phase-stable dual-comb interferometer," Nat. Commun. **9**(1), 1–7 (2018).